



# **Electrodeposition of Molybdenum from Water-in-Acetate Electrolytes**

Quanhong Liu and Qiang Huang\*, 2 [1]

Department of Chemical and Biological Engineering, University of Alabama, Tuscaloosa, Alabama 35487, United States of America

This paper reports a systematic study on the electrodeposition of metallic molybdenum from water-in-salt electrolytes containing superhigh concentrations of acetate. Cyclic voltammetry and DC deposition were carried out on rotating disk electrodes with various concentrations of CH<sub>3</sub>COOK and CH<sub>3</sub>COONH<sub>4</sub> to determine the effects of NH<sub>4</sub><sup>+</sup> and K<sup>+</sup> on Mo deposition. A comparison was performed between CH<sub>3</sub>COOLi, CH<sub>3</sub>COONa, and CH<sub>3</sub>COOK to study the effects of different alkali metal cations. A synergistic effect was observed between K<sup>+</sup> and NH<sub>4</sub><sup>+</sup>, where Mo deposition rate is enhanced in the presence of both cations. However, such synergistic effect was not observed between NH<sub>4</sub><sup>+</sup> and other alkali cations. In addition, the impact of substrate on Mo deposition was also studied using Pt and Cu electrodes with different activity toward hydrogen evolution reaction. Electron microscopy, X-ray diffraction, and X-ray photoelectron spectroscopy were used to characterize the surface morphology, crystallographic structure, and metallic state of Mo in the electrodeposited films.

© 2024 The Electrochemical Society ("ECS"). Published on behalf of ECS by IOP Publishing Limited. [DOI: 10.1149/1945-7111/

© 2024 The Electrochemical Society ("ECS"). Published on behalf of ECS by IOP Publishing Limited. [DOI: 10.1149/1945-7111/ad59c8]

Manuscript submitted February 12, 2024; revised manuscript received May 10, 2024. Published June 27, 2024.

Supplementary material for this article is available online

Molybdenum is attractive to the manufacturing industry, such as automotives, aeronautics, microelectronics, and semiconductors due to its high melting point, extremely low thermal expansion, and low electric resistance. <sup>2-4</sup> Generally speaking, metallic Mo coatings can be produced using thermal spraying, sintering, and pressing at high temperatures. <sup>5-7</sup>

Electrodeposition has been commonly used as a low-temperature process to prepare metal and alloy films using electrolytes. Compared with other types of electrolytes, aqueous solutions are nonflammable, easily prepared, and therefore of interest to most practical applications. However, metallic molybdenum is very difficult to deposit from aqueous solutions due to its highly negative reversible potential and, more importantly, the catalytic effect of the metal and various oxides toward hydrogen evolution reaction.8 Galvanic deposition can be used to fabricate Mo coating on Al alloy, resulting from a displacement reaction, where Al is oxidized to provide the electrons. 11 Electrodeposited Mo has also been reported. However, hazardous hydrofluoric acid electrolytes are used to avoid oxide formation <sup>12</sup> or an annealing process in a reducing atmosphere is used to convert the deposited oxide to metallic Mo. <sup>13</sup> Another way of electrodepositing Mo from aqueous solution is to co-deposit it with other transition metals, often an iron-group metal, leveraging the so-called induced electrodeposition mechanism. 14-17 However, such processes result in alloys rather than elemental Mo.

To the best of our knowledge, the only aqueous electrolyte system that has been used to successfully deposit Mo is based on an early study by Ksychi and Yntema, <sup>18</sup> where they reported that molybdenum can be electrodeposited from aqueous solutions containing superhigh concentrations of formate, acetate, propionate, fluoride, or phosphate salts. While there have been several recent studies focusing on the application of such electrolytes to electrodeposit thick Mo coatings, <sup>19–22</sup> the roles of different solutes and the effects of their concentration on Mo deposition have never been studied.

On the other hand, highly concentrated electrolytes can be categorized as the so-called water-in-salt electrolytes, a term emerged recently as opposed to the conventional salt-in-water electrolytes, describing the aqueous electrolytes where the free water molecules are effectively depleted due to the hydration of a superhigh concentration of salt.<sup>23,24</sup> While water-in-salt can fall under an even broader concept of solvent-in-solute system,<sup>25</sup> it

provides unique advantages to an aqueous solution. Not only does the electrolyte viscosity significantly increase but also the hydrogen bond network present in free water or dilute solutions is disrupted, resulting in a much lower rate of proton diffusion, slower hydrogen evolution reaction, and often a wider practical potential window for electrochemical applications. <sup>26,27</sup> The concept of water-in-salt was first introduced for lithium ion batteries, <sup>24</sup> and has been quickly and widely explored for other energy storage devices <sup>28</sup> and for electrodeposition applications. <sup>29–32</sup> Although Li<sup>+</sup> cation has been often used as a relatively strong Lewis acid to disrupt the hydrogen bond network, other salts or cations such as Na<sup>+</sup>, Zn<sup>2+</sup>, and K<sup>+</sup> have also been shown to have similar effects, albeit weaker. <sup>33–35</sup>

The early success on Mo deposition relied on the use of highly concentrated carboxylate aqueous solution.<sup>18</sup> However, the role of this high concentration of carboxylate salts or the so-called water-insalt property is not well studied. This work attempts to provide such understanding by performing a systematic study on molybdenum electrodeposition using acetates. While the anions can also play a role in the hydration of salt and impact the electrochemical behavior of electrolytes, their effects are strongly dependent on the charge density.<sup>36</sup> The monocharged bulky carboxylate anions have a low charge density and the impact on electrolyte is dominated by the cations. In this study, electrolytes with different ratios between the two acetates are used to investigate the contributions from the K+ and NH<sub>4</sub><sup>+</sup> cations. Sodium acetate and lithium acetate are also used to further determine the effects of alkali cations in these water-inacetate solutions on Mo deposition. The effects of metal substrate are also investigated.

# **Experimental**

Materials and chemical.—Sodium molybdate dihydrate, (Alfa Aesar, 99%), potassium acetate (Alfa Aesar, 99%), lithium acetate (Thermo Fisher, 99%), sodium acetate (Alfa Aesar, 99%), and ammonium acetate (Alfa Aesar, 99%) are used as received to prepare electrolytes for the studies. The molybdate concentration is kept at 0.02 M throughout the study, and the total acetate concentration are fixed at 9 M. Various concentrations of potassium acetate from 9 to 0 M, are used. At the same time, the concentration of ammonium acetate is changed from 0 to 9 M accordingly. Similar electrolytes with total acetate at 9 M are also prepared using sodium acetate and lithium acetate. However, the upper limit concentrations are 3 M and 4.5 M for sodium acetate and lithium acetate, respectively, above which the salt is not completely dissolved. At the same time, the concentration of ammonium acetate decreases

<sup>\*</sup>Electrochemical Society Member.

<sup>&</sup>lt;sup>z</sup>E-mail: qhuang@eng.ua.edu

from 9 M to a lower limit of 6 M and 4.5 M, respectively. All electrolytes were prepared using deionized (DI) water with a resistivity of 18 M $\Omega$ -cm. While an elevated temperature of 30 °C may be used to speed up salt dissolution during electrolyte preparation, all studies are carried out at a room temperature of 20 °C. All electrolytes are kept at natural pH (between 7.2 to 10.1).

Electrochemical cell.—A traditional electrochemical cell with three compartments is used in all studies. The reference electrode is a silver chloride (Ag/AgCl) electrode saturated with KCl (0.197 V vs NHE) in the reference compartment connected to the catholyte through a capillary. All potentials are referred with respect to this electrode in this work. A 99.99% platinum foil is used as the counter electrode in the anolyte compartment separated from the catholyte with a glass frit. Three different substrates are used in this study. The electrochemical studies, such as cyclic voltammetry and anodic stripping analysis, are carried out on a Pt rotating disc electrode (RDE) and Cu pre-plated Pt RDE with a diameter of 5 mm or a surface area of 0.196 cm<sup>2</sup>. A layer of Cu is pre-plated on Pt RDE in some electrochemical studies using a Cu make up electrolyte at -20mA cm<sup>-2</sup> for 20 s. The Cu electrolyte comprises 0.63 M CuSO<sub>4</sub>, 0.1 M H<sub>2</sub>SO<sub>4</sub>, and 1 mM KCl. In addition, Cu disks are used for DC deposition to prepare Mo films for material characterization. The RDE rotation rate in all studies is fixed at 1000 rpm.

Instruments and procedures.—The dynamic viscosity of electrolytes is measured at room temperature using a Viscolite 700HP laboratory viscometer system with a HP550 signal processor, corrected with the solution density determined using a Mettler Toledo balance. An Autolab 302 N potentiostat with frequency analyzer is used for all electrochemical studies. The effects of substrate and acetate concentration are studied using cyclic voltammetry. Direct-current (DC) deposition is caried out at different potentials using the chronoamperometry method. The thickness of deposited films is measured with a Bruker M1 Mistral X-ray fluorescence spectroscope (XRF) with a 0.7 mm collimator operated at 50 kV. Five spots on the surface evenly across the diameter of RDE are selected for XRF measurements. The average thickness across these five locations is reported. The deposited metal on Pt RDE is also anodically stripped. The total stripping charge is compared against the film thickness from XRF measurements to calibrate the number of electrons transferred during anodic stripping, i.e., the valence of dissolved Mo species upon stripping. The film morphology is characterized with a Thermo Fisher Apero Field Emission Scanning Electron Microscope (FE-SEM) operated at 20 kV. The crystallographic structure of the deposited films is determined using a Philips XPert Materials Diffractometer with a 45 kV, 40 mA Cu K $\alpha$  radiation (wavelength = 1.54 Å). The X-ray photoelectron spectroscopy (XPS) characterization of the deposit is performed using a Phi Physical Electronics VersaProbe 5000 XPS spectrometer with a monochromatic Al K $\alpha$ X-ray source.

### **Results and Discussion**

*Electrochemical study.*—Cyclic voltammetry (CV) is first carried out to study Mo electrodeposition using an electrolyte with 4.5 M CH3COOK and 4.5 M CH3COONH4. Figure 1a shows a set of CVs conducted on the Cu pre-plated RDE with different cathodic vertex potentials. A rotation rate of 1000 rpm and a scan rate of 20 mV sec<sup>-1</sup> are used. A much narrower CV with a cathodic vertex of -0.8 V before cathodic current emerges is included for comparison, where only a single anodic peak of Cu stripping is observed starting at -0.1 V. As the cathodic vertex reaches -2.0 V, multiple changes can be observed in the CVs. First, an additional anodic peak emerges at -0.3 V, corresponding to the stripping of electrodeposited film. As Fig. 1b shows, this threshold voltage for cathodic deposition becomes -1.3 V after the correction of solution ohmic drop. Furthermore, a third anodic peak is observed at +0.3 V when the

cathodic potential reaches  $-2.8\,\mathrm{V}$ , or  $-1.5\,\mathrm{V}$  after ohmic drop correction, suggesting another Mo species in the deposit being anodically stripped. The amount of deposited Mo continues to increase as the cathodic vertex potential becomes more negative. An extremely high cathodic current density is obtained for all CVs, suggesting a very strong hydrogen evolution rate and a very low current efficiency for Mo deposition.

A same set of CVs acquired on Pt RDE with different cathodic vertex potentials are presented in Fig. S1 in Supplementary Materials. While these anodic stripping peaks are also observed, the peaks emerge when the cathodic sweeps reach more negative potentials than on Cu RDE and the peaks are less significant. The stripping charges of Mo are calculated by integrating all the anodic peaks for each CV and are presented in Table S1 in Supplementary Materials to provide a more direct comparison between the two substrates. The stripping charge of the Cu layer is subtracted from the total stripping charge when the Cu pre-plated RDEs are used. It is evident that more Mo is deposited on Cu than on Pt. A difference of about 70 mC cm<sup>-2</sup> stripping charge is observed between Cu and Pt substrates regardless of the cathodic vertex potential, namely, how long the cathodic deposition lasts. Figure 1c shows a magnified comparison between the Pt and Cu substrates at the early portion of cathodic sweeps, with and without ohmic drop correction. The cathodic current is much higher on Pt than on Cu at the same potential, corresponding to a facilitated hydrogen evolution reaction. This expedited side reaction appears to not only suppress Mo deposition for the first few layers but also prevent the formation of a continuous film on Pt surface, thus extending the effects beyond the early stage of deposition.

Mo oxidation may produce oxide species, such as MoO<sub>2</sub>,<sup>37</sup> passivating the surface until a higher anodic potential is reached to further strip it in a form of HMoO<sub>4</sub><sup>-</sup> or MoO<sub>4</sub><sup>2-</sup> depending on the electrolyte pH. As the CV in Fig. 1a shows, when the cathodic vertex reaches below -2.3 V, a fourth anodic current peak is observed at 0 V in the cathodic sweep after anodic sweep. This anodic peak on the cathodic sweep is not observed on Pt RDEs in Fig. S1, suggesting that it can be attributed to the passivation of Cu at highly positive potentials in this electrolyte, preventing the dissolution until the potential sweeps back to a moderate 0.1 V. This incomplete stripping of Cu is further exacerbated by the Mo capping electrodeposited on Cu. Detailed CV studies with a prolonged stripping at a moderately positive potential have been designed to confirm this hypothesis.

Figure 2 shows three CVs conducted on Cu pre-plated Pt RDE between -2.8 to 0.8, similar to the green CV in Fig. 1b. Two of the them include an additional 80 s hold at 0.1 V and 0.3 V, respectively. The third CV without any hold is presented for comparison, where a clear anodic peak is observed on the cathodic sweep after the anodic vertex, same as the observation in Fig. 1b. When a potentiostatic hold at 0.1 V is added into the anodic sweep, as shown in Fig. 2a, the current decays to 0 upon the hold. No anodic peak is observed in the cathodic sweep, suggesting that all metals are completely stripped and Cu passivation does not occur. On the other hand, when a more positive potential of 0.3 V is used for the hold, as shown in Fig. 2b, the current decays more slowly reaching a small yet positive value after 80 s and a small anodic peak remains in the reverse scan. This suggests that Cu passivation occurs at this more positive potential of 0.3 V and complete dissolution is not achieved until the potential sweeps back to the moderately positive 0.1 V.

To further investigate the effects of electrolyte chemistry on Mo deposition, the same CV studies are carried out using electrolytes with various concentrations of CH<sub>3</sub>COOK. A fixed rotation rate of 1000 rpm, a fixed scan rate of 20 mV s $^{-1}$ , and a fixed potential range of -2.8 to +1.0 V are used. Figure 3a shows the CVs on Cu preplated RDE and Fig. 3b shows the same CVs after the correction of solution resistance. The stripping curve of the pre-plated Cu layer performed in the solution with 4.5 M CH<sub>3</sub>COOK is included for comparison. The anodic stripping current peak between -0.3 to +0.5 V becomes more pronounced as the concentration increase

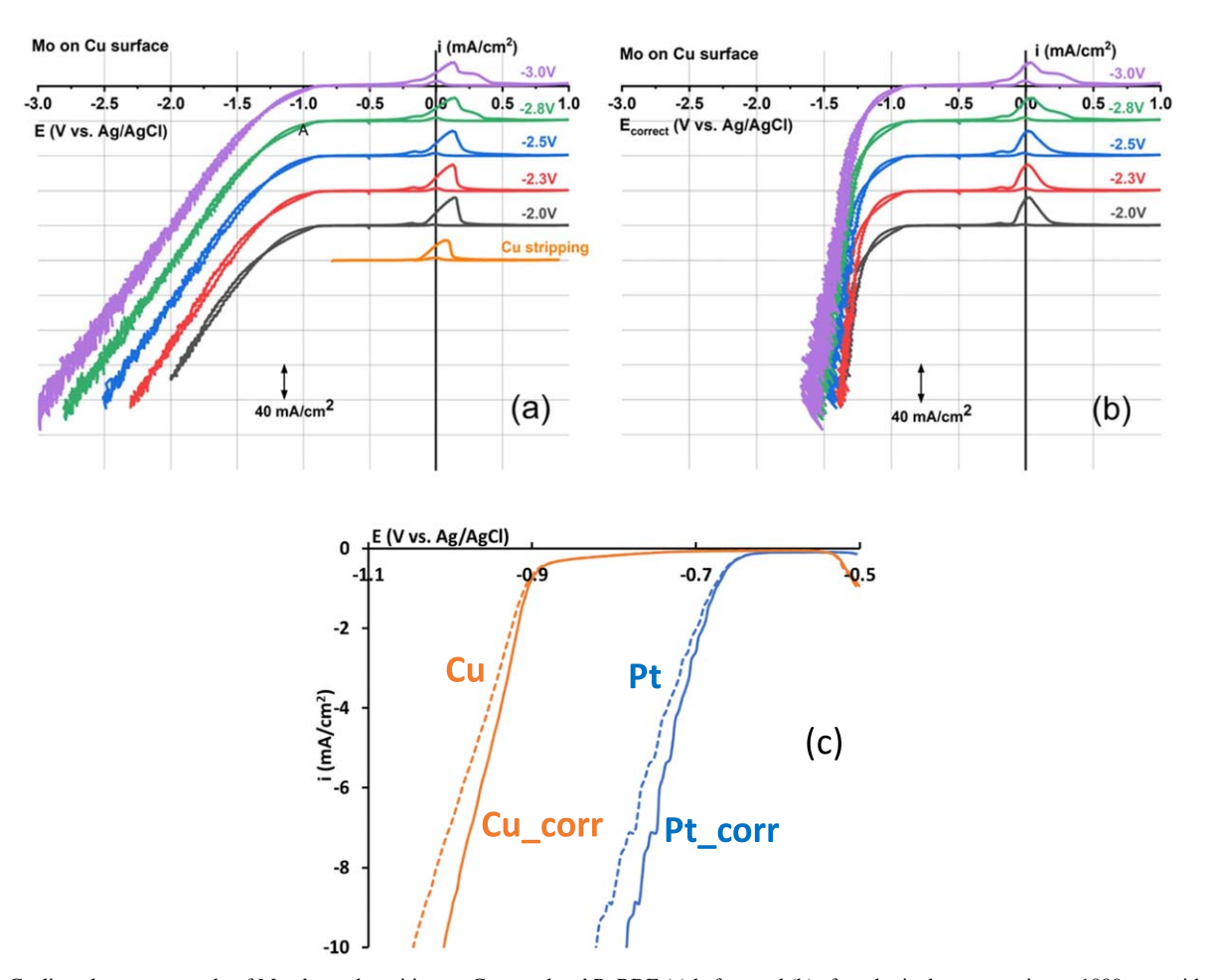


Figure 1. Cyclic voltammetry study of Mo electrodeposition on Cu pre-plated Pt RDE (a) before and (b) after ohmic drop correction at 1000 rpm with different cathodic potential vertices in the electrolyte containing 0.02 M MoO<sub>4</sub> $^{2-}$ , 4.5 M CH<sub>3</sub>COOK, and 4.5 M CH<sub>3</sub>COONH<sub>4</sub>. The anodic stripping of pre-plated Cu layer in the same electrolyte is included for comparison. Scan rate is  $20 \text{ mV} \text{ s}^{-1}$ . (c) A magnified comparison of cathodic sweeps at low current densities on Pt and Cu pre-plated RDEs before and after ohmic drop correction.

from 1 M to 6 M, above which it becomes much smaller. The impedances of the different solutions are listed in Table S2 in Supplementary Materials. They are almost identical with an average impedance of 18.1 ohm and a deviation of 1.5 ohm. Therefore, the potential range after the correction of ohmic drop are still similar for different CVs and the different anodic stripping peaks observed are due to the impact of solution chemistry.

A same set of CV studies are also carried out on Pt RDE and the results are shown in Fig. S2 in Supplementary Materials. The presence of CH<sub>3</sub>COOK is also found beneficial for Mo deposition on Pt. First, anodic stripping peak is not observed until the CH<sub>3</sub>COOK concentration reaches 4.5 M. Second, the anodic stripping peak continues to increase with the CH<sub>3</sub>COOK concentration up to 6 M. The stripping charges of Mo deposited from different electrolytes are also integrated from the CV results and are summarized in Table S2 in Supplementary Materials to provide a direct comparison between Pt and Cu pre-plated RDEs. The net charge of Mo stripping is calculated by subtracting Cu stripping from the total stripping charge. Only one stripping curve of the preplated Cu layer performed in the solution with 4.5 M CH<sub>3</sub>COOK is presented in the Fig. 3a. However, such stripping studies have been conducted in different solutions, i.e. from 1 to 8 M CH<sub>3</sub>COOK, and the stripping behaviors of the Cu layer are nearly identical with an average integrated charge of 254.5 mC cm<sup>-2</sup> and a 2.6% standard deviation, i.e. 6.7 mC cm<sup>-2</sup>, between the six solutions. This deviation is negligible compared with the net stripping charge of Mo deposits. It is evident from the stripping charges that more Mo is deposited on Cu surface than on Pt, consistent with the observation

in Fig. 1. On the other hand, the stripping charge of Mo increases with CH<sub>3</sub>COOK concentration up to 6 M, above which the amount of Mo sharply decreases to nearly null at 8 M. It is also worth noting that the net stripping charge difference between Pt and Cu substrates in Table S2 is not a constant when the electrolyte changes. This is in contrast to the observation in Fig. 1, where a single solution is used. While the gas evolution side reactions are more facilitated on Pt than Cu, suppressing Mo deposition, the significance of this contrast between Pt and Cu appears to be different in different electrolytes.

In order to further clarify the effects of potassium acetate on Mo deposition behavior along different potentials, DC electrodeposition is carried out at different constant potentials in the electrolytes with various concentrations of CH<sub>3</sub>COOK from 0 to 9 M. The total acetate concentration (CH3COOK and CH3COONH4) is still fixed at 9 M. The deposited films are stripped using an anodic sweep at a rate of 1 mV sec<sup>-1</sup>. As discussed in Fig. 2, this sweep rate is sufficiently slow to avoid Cu passivation at highly positive potential before complete dissolution. The stripping charge of a pre-plated Cu layer is subtracted from the Mo stripping charge. The valence of stripped Mo is first confirmed to be +6 by comparing the film thickness measured with XRF and the Mo stripping method. The current efficiencies are calculated as the ratio between Mo stripping charge and the cathodic DC deposition charge and are presented as Table S3 in Supplementary Materials. While the efficiency increases with the CH<sub>3</sub>COOK concentration, it remains below 2.6% regardless of the electrolytes and deposition potentials. Figure 4 summarizes the partial current densities calculated from the Mo stripping charge. As Fig. 4a shows, the partial current density of Mo deposition on Pt

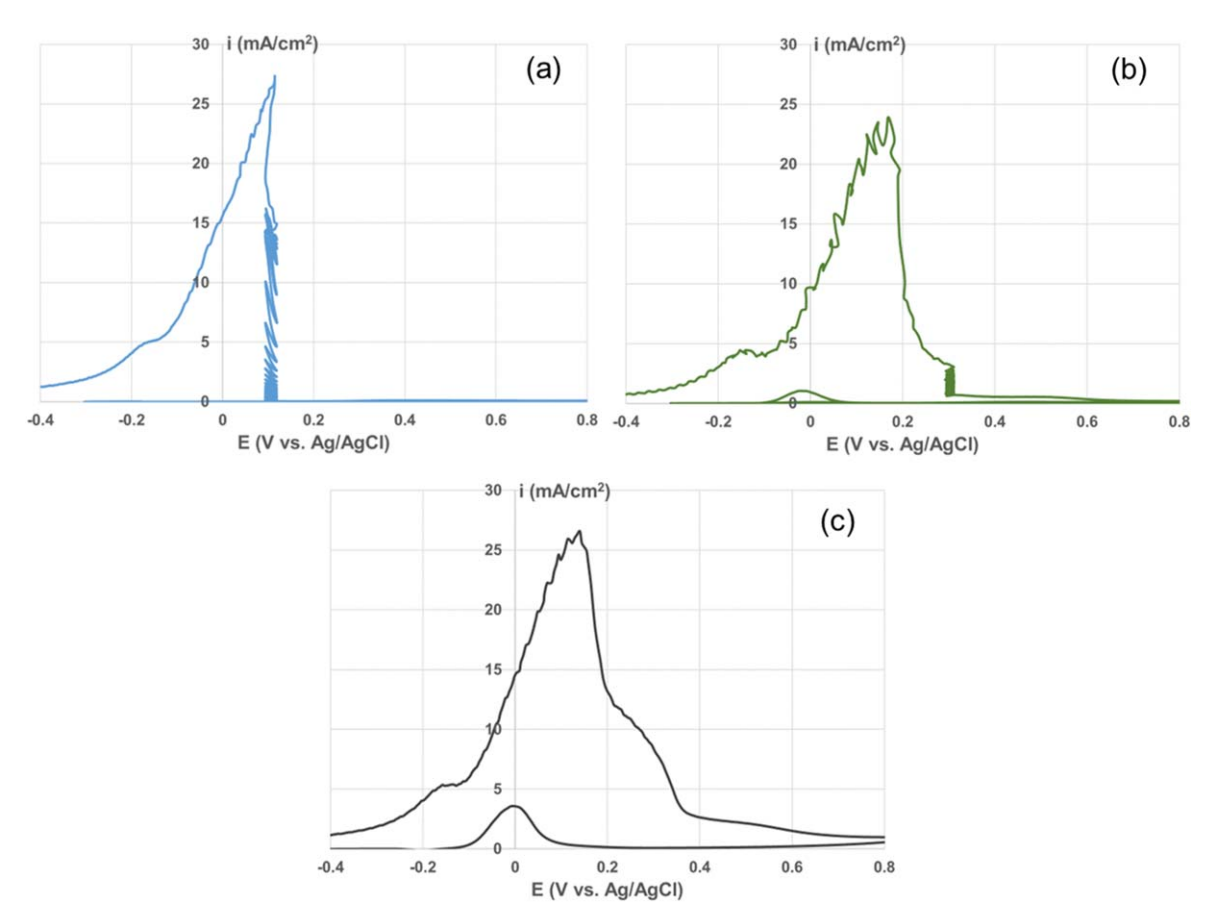


**Figure 2.** Anodic portions of three cyclic voltammetry studies with an identical cathodic sweep to -2.8 V on a Cu pre-plated RDE at 1000 rpm. The potential on the anodic scan was held at (a) 0.1 V and (b) 0.3 V for 80 s, and (c) without potential hold. The scan rate is 20 mV s<sup>-1</sup> for all cases. The solution contains 0.02 M  $MoO_4^{2-}$ , 4.5 M  $CH_3COOK$ , and 4.5 M  $CH_3COONH_4$ .

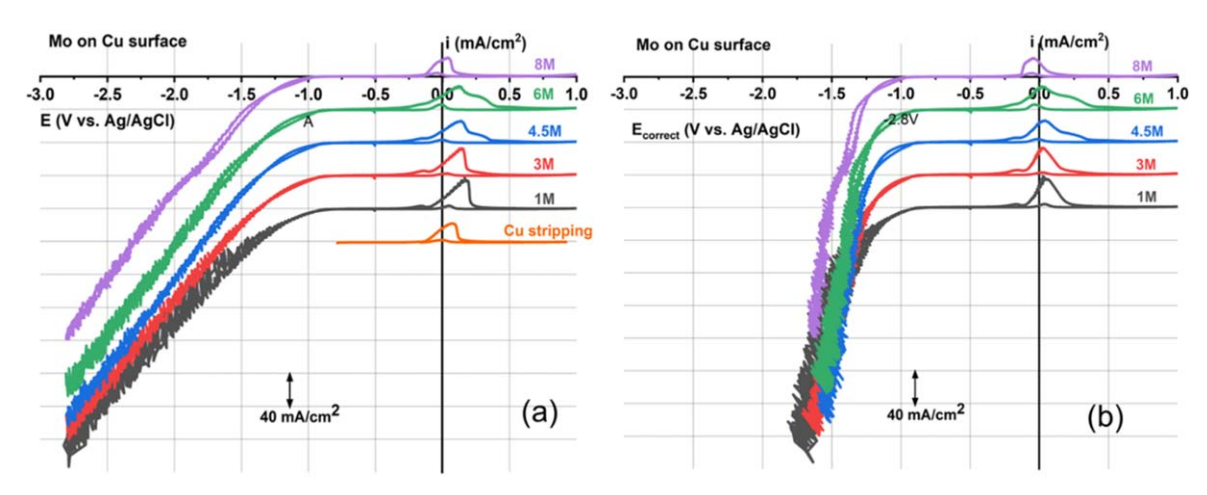


Figure 3. Cyclic voltammetry study of Mo electrodeposition on Cu pre-plated RDE (a) before and (b) after ohmic correction at 1000 rpm in electrolytes with different CH<sub>3</sub>COOK concentrations. The total acetate concentration is 9 M. Scan rate is  $20 \text{ mV s}^{-1}$ . The stripping of pre-plated Cu layer in the  $4.5 \text{ M CH}_3$ COOK electrolyte is included in for comparison.

remains under 3 mA cm $^{-2}$  across all the electrolytes and potentials studied. However, it becomes significantly higher on Cu pre-plated RDE. The maximum current density of Mo deposition on Cu reaches above 8 mA cm $^{-2}$ , which almost triples the maximum rate on Pt. The Mo deposition rate on Pt showed no clear trend as the K $^+$  concentration increases from 0 to 6 M regardless of the correction of ohmic drop. No Mo deposition is obtained when K $^+$  concentration is 8 M or higher. On the other hand, Mo deposition rate on Cu clearly increases with K $^+$  concentration up to 6 M. This increasing trend

becomes even more pronounced after the potentials are corrected with the ohmic drops. Same as the case on Pt, no Mo films are obtained when the electrolytes containing 8 M or more potassium acetate regardless of the potentials. On contrary, Mo can be deposited with 8 M CH<sub>3</sub>COONH<sub>4</sub> or more. Therefore, while the presence of CH<sub>3</sub>COOK may facilitate Mo electrodeposition on Cu, more than 1 M CH<sub>3</sub>COONH<sub>4</sub> is necessary for Mo deposition regardless of the electrode metal speciation.

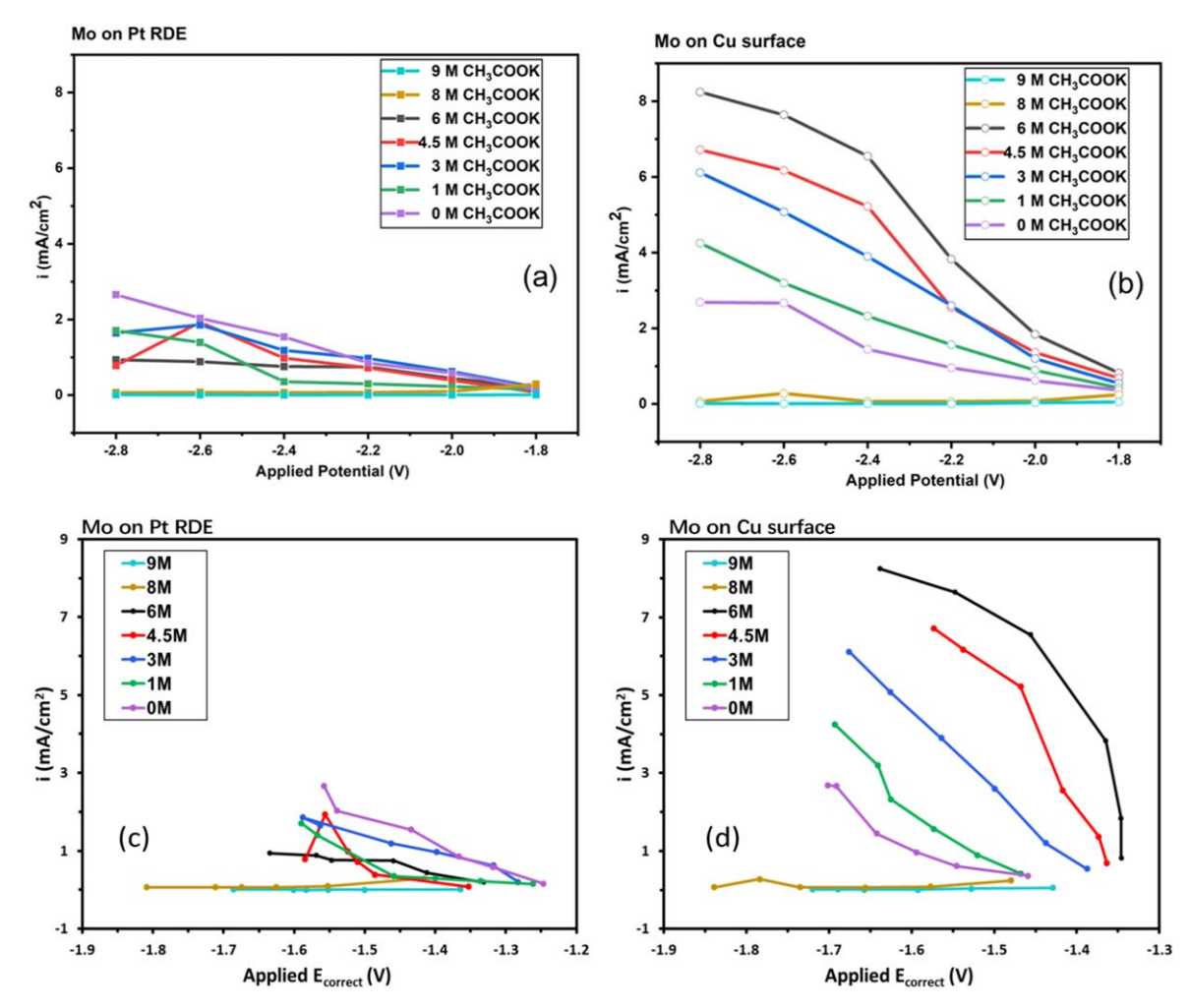


Figure 4. Partial current densities of DC deposition of Mo at different constant potentials on (a), (c) Pt RDE and (b), (d) Cu-preplated Pt RDE at 1000 rpm in solutions with various CH<sub>3</sub>COOK concentrations (a), (b) before and (c), (d) after ohmic drop correction.

Some reasons can contribute to the observations above. CH<sub>3</sub>COONH<sub>4</sub> is a good pH buffer, where the NH<sub>4</sub><sup>+</sup> at a sufficiently high concentration is expected to interact with the OH<sup>-</sup> byproduct during Mo deposition, stabilizing the surface pH. A higher surface pH would otherwise facilitate the formation of various Mo oxides, further promoting hydrogen evolution and water reduction and preventing Mo deposition. 19 On the other hand, CH<sub>3</sub>COOK itself does not have buffering capacity around the neutral pH used in this study. Therefore, a minimum CH<sub>3</sub>COONH<sub>4</sub> concentration is necessary for Mo deposition and a high concentration of CH<sub>3</sub>COOK alone with little to no NH<sub>4</sub><sup>+</sup> results in no deposition. On the other hand, the observation clearly shows a synergistic effect between K<sup>+</sup> and NH<sub>4</sub><sup>+</sup> for Mo deposition, where the Mo deposition rate is significantly facilitated by a high concentration of K<sup>+</sup> in addition to CH<sub>3</sub>COONH<sub>4</sub>. Several mechanisms may potentially contribute to this synergy. First, the dynamic viscosity of electrolytes containing different concentrations of CH3COOK is also listed in Table S3 in Supplementary Materials. The viscosity of the solution increases with the CH<sub>3</sub>COOK concentration, which further slows down the movement of ions including protons. Second, the different concentrations of potassium acetates also change the initial bulk pH and the buffering capacity of solution, impacting Mo deposition behavior. The third potential reason is the "water-in-salt" effect. K<sup>+</sup> is a monovalent cation with a higher charge density than NH<sub>4</sub><sup>+</sup> and is expected to provide more pronounced "water-in-salt" characteristics to the solution than  $\mathrm{NH_4}^{+38,39}$  For example, Chen et al. analyzed the FTIR and Raman spectra of water molecules near the electrode surface, which suggests that the water molecules in the hydration

sheath of  $K^+$  ions can be shared between multiple  $K^+$  ions, forming a continuous chain structure with water molecules bridging between the  $K^+$  ions. When the structure with water molecules bridging tetrahedral hydrogen bond network among free water molecules, namely, the "water-in-salt" effect.

Additional studies are conducted on Mo deposition using Li<sup>+</sup> and Na<sup>+</sup> acetates to further determine the significance of the "water-insalt" effect on Mo deposition. Figures 5a and 5b show the dependence of Mo deposition partial current density on the applied potential in similar acetate electrolytes but with various concentrations of CH<sub>3</sub>COOLi and CH<sub>3</sub>COONa instead of CH<sub>3</sub>COOK. The maximum concentration of CH<sub>3</sub>COONa and CH<sub>3</sub>COOLi is 3 M and 4.5 M, respectively, due to the limitation of solubility in this electrolyte system. The Mo deposition rate in Fig. 5a decreases as CH<sub>3</sub>COONa concentration increases from 0 to 3 M regardless of the deposition potential. A similar decreasing trend is also observed for CH<sub>3</sub>COOLi in Fig. 5b. In addition, Fig. 5c summarizes the partial current density at -2.8 V as a function of the concentration of different alkali metal cations. It is evident that the Mo deposition rate in CH<sub>3</sub>COONa electrolyte is much lower than the cases with CH<sub>3</sub>COOK, and the rate with CH<sub>3</sub>COOLi is even lower. More importantly, the addition of Li<sup>+</sup> and Na<sup>+</sup> suppresses Mo deposition and this suppression monotonically intensifies as the concentration increases. This is in contrast to K<sup>+</sup>, which promotes Mo deposition as the concentration increases until 6 M, above which Mo deposition is completely disabled probably due to insufficient pH buffering from CH<sub>3</sub>COONH<sub>4</sub>. The so-called water-in-salt effect becomes stronger as the charge density of cation increases or as the radius

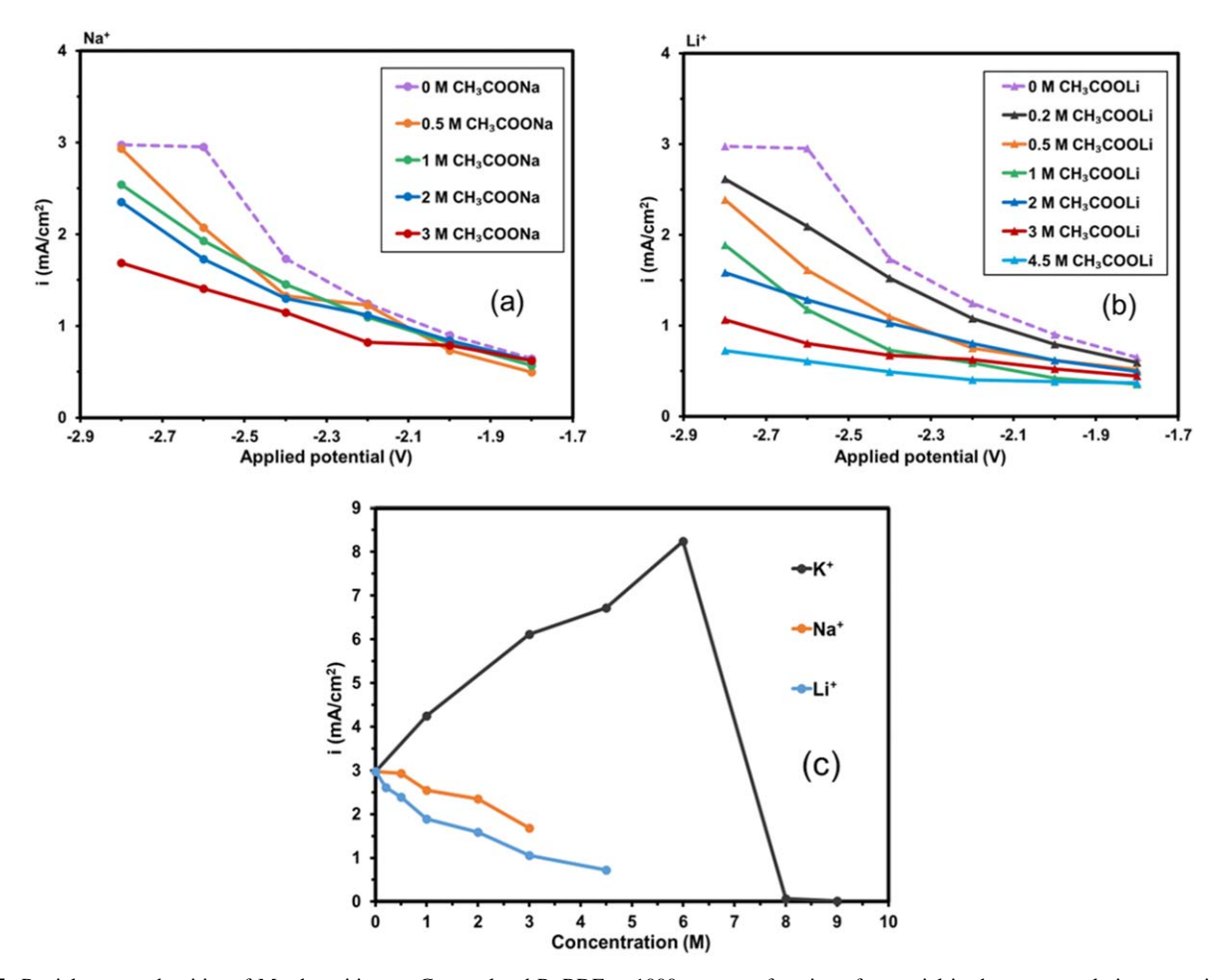


Figure 5. Partial current densities of Mo deposition on Cu-preplated Pt RDE at 1000 rpm as a function of potential in the acetate solutions contains various concentration of (a) CH<sub>3</sub>COONa and (b) CH<sub>3</sub>COOLi; and (c) the partial current density of Mo deposition at -2.8 V as a function of the concentration of different alkali metal cations up to their respective solubility. The total acetate concentration is fixed at 9 M. Purple dash lines in (a) and (b) represent the cases with 9 M CH<sub>3</sub>COONH<sub>4</sub> but no CH<sub>3</sub>COONa or CH<sub>3</sub>COOLi.

of alkali cation decreases.<sup>38</sup> While such stronger water-in-salt effects may have suppressed HER, it appears to inhibit Mo deposition in this study. In other words, the results in this set of study suggest the generic water-in-salt effect, or the disruption of hydrogen bond network by a strong Lewis acid, is not necessary or beneficial for Mo deposition.

Film characterization.—The morphology of electrodeposited Mo film is characterized with SEM. Figures 6a and 6b show the top-down SEM images of Mo films deposited on the Cu disc electrodes at a DC potential of -2.8 V for 900 s in solutions with 4.5 M and 6 M CH<sub>3</sub>COOK, respectively. The total acetate concentration is still maintained at 9 M using CH<sub>3</sub>COONH<sub>4</sub>. The morphology of the Cu disc substate is included in 6(c) for comparison. Visual inspection reveals smooth and shiny films with a silver-grey luster. The SEM images in (a) and (b) show coalescent films with nodules and cracks, consistent with previous studies.<sup>21</sup> These cracks result from a high internal stress in the deposited Mo films related to the strong side reactions at the highly negative potentials needed for Mo deposition. As a comparison, the morphology of a Mo film deposited on Pt at the same conditions as Fig. 6a is presented in Fig. S3 in the Supplemental Materials. The deposit on Pt appears discontinuous by visual inspection and the SEM image shows separated particles and patches with various sizes. This is also consistent with the much stronger hydrogen evolution and water reduction on Pt, suppressing or preventing Mo deposition as discussed above.

XRD is used to characterize the crystallographic structures of electrodeposited Mo films and the results are shown in Fig. 7. The films are deposited on Cu disk RDEs at various potentials from -2.1to  $-2.8 \, \text{V}^{-}$  for 900 s using an electrolyte containing 4.5 M CH<sub>3</sub>COOK and 4.5 M CH<sub>3</sub>COONH<sub>4</sub>. The film thickness is estimated between 290 to 1020 nm using the partial current densities in Fig. 4. The three strong peaks observed at  $2\theta$  of  $43.19^{\circ}$ ,  $50.30^{\circ}$ , and 73.8° correspond to the Cu substrate with large grains. Only a relatively broad peak at a  $2\theta$  of  $40.42^{\circ}$  is observed for the Mo(100) for all the potentials used. No peak indicative of molybdenum oxides is observed. The intensity and width of this Mo(100) peak remain relatively unchanged across the deposition potentials, corresponding to a grain size between 7 to 9 nm estimated using the Scherrer equation. It is noted that Mo(211), if present, overlaps with Cu(220) at the  $2\theta$  of  $74^{\circ}$  and may become obscure. After all, the XRD results indicate that metallic Mo could be deposited from acetate solution, albeit of a small grain size.

The as-deposited Mo coating is further characterized with X-ray photoelectron spectroscopy (XPS) to determine the metallic nature of deposit. Figure 8 shows the results for a film deposited at -2.8 V for 900 s with 4.5 M CH<sub>3</sub>COOK, a duplicate of the same films for SEM and XRD characterizations in Figs. 6a and 7. Two XPS spectra around the Mo binding energy are presented before and after sputter cleaning the surface. The carbon signal (C1) is used as a standard to calibrate the binding energy. For the as-deposited film, two metallic Mo peaks are observed at 227.4 eV and 230.5 eV, corresponding to Mo(0)  $3d_{5/2}$  and  $3d_{3/2}$ , respectively. However, not only are these two peaks weak but one additional peak is also observed, at 235.1 eV,

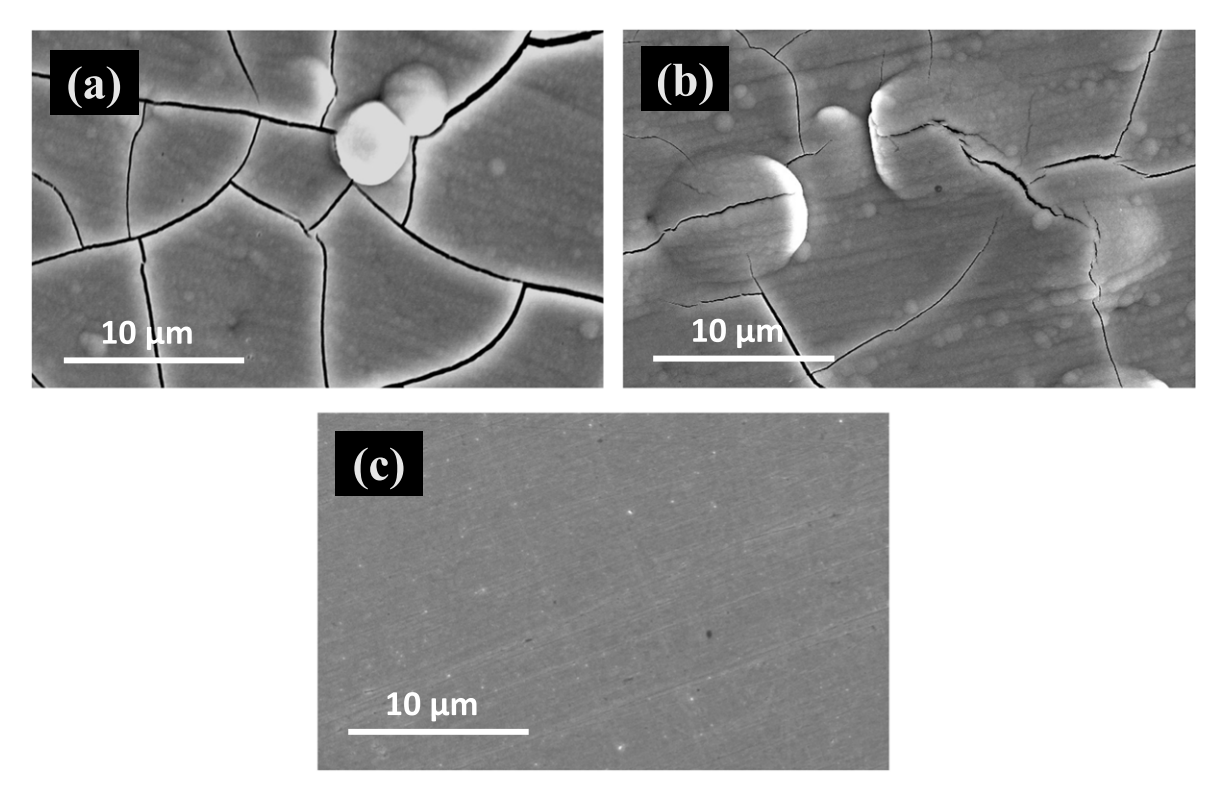


**Figure 6.** Top-down SEM images of Mo films deposited on Cu RDEs at 1000 rpm and −2.8 V from a solution with (b) 4.5 M and (c) 6 M CH<sub>3</sub>COOK, and (c) the surface of Cu RDE itself.

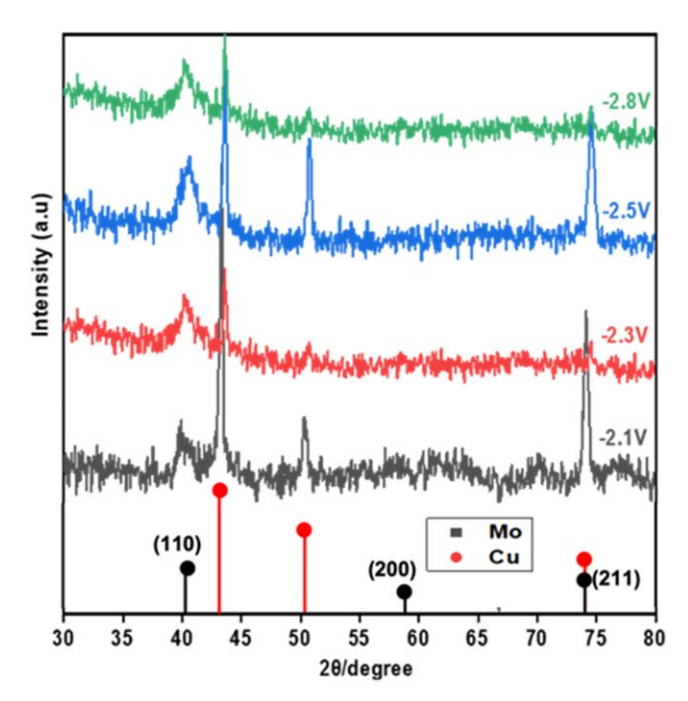


**Figure 7.** XRD patterns of Mo films deposited from  $4.5 \text{ M CH}_3\text{COOK}$  at various deposition potentials for 900 s on Cu pre-plated substrate, and XRD standards of Mo and Cu.

corresponding to the Mo(VI). <sup>41</sup> To eliminate the effects of surface oxidation of Mo, 20 s sputter cleaning is performed before another XPS analysis. The two metallic Mo peaks are significantly intensified after the cleaning and the Mo(VI) signal is diminished. The sputter cleaning process is estimated to remove about 2 to 5 nm materials off the top surface. This change in XPS clearly demonstrates that the majority of Mo(VI) species are surface oxides

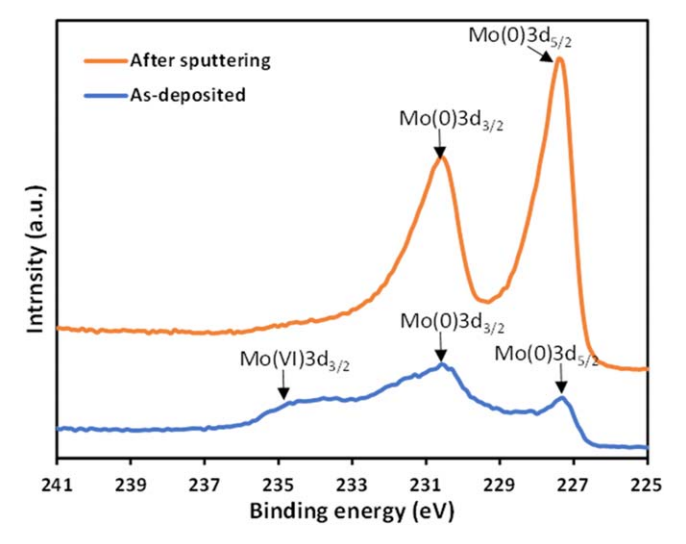


**Figure 8.** XPS spectrum around Mo 3d binding energy of Mo film electrodeposited at -2.8 V for 900 s on Cu pre-plated substrate from an electrolyte with 4.5 M CH<sub>3</sub>COOK and 4.5 M CH<sub>3</sub>COONH<sub>4</sub>. The spectra are acquired for an as-deposit film and the same film after sputter cleaning.

(MoO<sub>3</sub>) probably formed upon the exposure to ambient and the deposited film beneath the surface primarily consists of metallic Mo.

# Conclusions

The electrodeposition of elemental Mo films using water-in-salt electrolytes with superhigh concentrations of acetates is systematically studied. The as deposited films on Cu are metallic Mo with a nanocrystalline grain structure in a preferred (100) orientation. The Mo deposition rate on Pt surface is much suppressed compared with Cu surface across all the potentials due to the facilitated hydrogen evolution reactions on Pt, resulting in much thinner and non-

coalescent Mo films. No Mo can be electrodeposited regardless of substrates when the CH<sub>3</sub>COONH<sub>4</sub> concentration is 1 M or lower, probably relating to the pH buffering capacity required for mitigating surface pH increase, reducing oxide formation, and enabling Mo deposition. On the other hand, the Mo deposition rate in CH<sub>3</sub>COONH<sub>4</sub> electrolytes increases with the K<sup>+</sup> concentration up to 6 M. However, the use of other alkali metal cations, such as Li and Na<sup>+</sup>, in place of K<sup>+</sup> suppresses Mo deposition, suggesting that the generic water-in-salt effect from the disruption of hydrogen bond network at an extremely high ionic concentration is not beneficial for Mo deposition. The promoted Mo deposition rate at 6 M CH<sub>3</sub>COOK suggests a specific synergistic effect between CH<sub>3</sub>COOK and CH<sub>3</sub>COONH<sub>4</sub>.

#### Acknowledgments

National Science Foundation is acknowledged for support through a grant 1941820. The Alabama Analytical Research Center, College of Engineering Analytical Facility, and A&S glass shop at the University of Alabama are acknowledged for characterization and for making the parts used in this study. Dr. Paul Baker at the Center for Nanoscale Materials and Biointegration at University of Alabama Birmingham is gratefully acknowledged for training and assistance during the XPS characterization.

## **ORCID**

Qiang Huang https://orcid.org/0000-0002-1391-6531

# References

- 1. G. Jin, B. S. Xu, H. D. Wang, Q. F. Li, and S. C. Wei, "Tribological properties of molybdenum coatings sprayed by electro-thermal explosion directional spraying." Surf. Coat. Technol., 201, 6678 (2007).
- 2. M. Laribi, A. B. Vannes, and D. Treheux, "Study of mechanical behavior of molybdenum coating using sliding wear and impact tests." Wear, 262, 1330 (2007).
- 3. A. Fernández Guillermet, "Critical evaluation of the thermodynamic properties of molybdenum." Int. J. Thermophys., 6, 367 (1985).
- 4. E. I. Steifel, "Molybdenum and Molybdenum Alloys." Kirk-Othmer Encyclopedia of Chemical Technology 1.
- 5. H. S. Huang and K. S. Hwang, "Deoxidation of molybdenum during vacuum sintering." Metall. Mater. Trans. A, 33, 657 (2002).
- 6. M. V. Babu, R. K. Kumar, O. Prabhakar, and N. G. Shankar, "Simultaneous optimization of flame spraying process parameters for high quality molybdenum coatings using Taguchi methods." *Surf. Coat. Technol.*, **79**, 276 (1996).
- 7. A. Vaidya, T. Streibl, L. Li, S. Sampath, O. Kovarik, and R. Greenlaw, "An integrated study of thermal spray process-structure-property correlations: a case study for plasma sprayed molybdenum coatings." Mater. Sci. Eng., A, 403, 191 (2005)
- 8. R. K. Shervedani and A. Lasia, "Study of the hydrogen evolution reaction on Ni-Mo-P electrodes in alkaline solutions." J. Electrochem. Soc., 145, 2219 (1998).
- J. C. Padilha, E. M. A. Martini, C. Brum, M. O. de Souza, and R. F. de Souza, "Study of molybdenum electrodes for hydrogen evolution reaction." J. Power Sources, 194, 482 (2009).
- 10. A. J. Bard, R. Parsons, and J. Jordan, Standard Potentials in Aqueous Solution (Marcel Dekker Inc, New York) (1985).
- 11. B. D. Falola, A. Krishnamurthy, R. Radhakrishnan, and I. I. Suni, "Galvanic deposition of Mo Atop Al 6061 alloy." ECS Electrochem. Lett., 2, D37 (2013).
- 12. N. D. Ivanova, S. V. Ivanov, E. I. Boldyrev, and O. A. Stadnik, "Electrodeposition of metal molybdenum from electrolytes containing hydrofluoric acid." Prot. Met., **42**, 354 (2006).
- 13. R. S. Patil, M. D. Uplane, and P. S. Patil, "Structural and optical properties of electrodeposited molybdenum oxide thin films." Appl. Surf. Sci., 252, 8050 (2006).
- 14. N. Eliaz and E. Gileadi, "Induced codeposition of alloys of tungsten, molybdenum and rhenium with transition metals." Modern Aspects of electrochemistry (Springer New York)191 (2008).

- 15. E. Gomez, E. Pellicer, and E. Valles, "Influence of the bath composition and the pH on the induced cobalt-molybdenum electrodeposition." J. Electroanal. Chem., 556,
- 16. E. J. Podlaha and D. Landolt, "Induced codeposition.1. an experimental investigation of Ni-Mo alloys." J. Electrochem. Soc., 143, 885 (1996).
- 17. Y. Zeng, M. Ma, X. M. Xiao, Z. L. Li, S. X. Lian, and S. M. Zhou, "Kinetic model of induced codeposition of Ni-Mo alloys." Chin. J. Chem., 18, 29 (2000).
- 18. M. J. Ksycki and L. F. Yntema, "The electrodeposition of molybdenum from aqueous solutions." J. Electrochem. Soc., 96, 48 (1949).
- 19. T. J. Morley, L. Penner, P. Schaffer, T. J. Ruth, F. Bénard, and E. Asselin, "The deposition of smooth metallic molybdenum from aqueous electrolytes containing molybdate ions." Electrochem. Commun., 15, 78 (2012).
- R. Syed, S. K. Ghosh, P. U. Sastry, G. Sharma, R. Hubli, and J. K. Chakravartty, "Electrodeposition of thick metallic amorphous molybdenum coating from aqueous electrolyte." Surface & Coatings Technology, 261, 15 (2015).
- 21. A. Haftbaradaran, N. Parvini-Ahmadi, and S. Yazdani, "Electrodeposition and characterization of metallic molybdenum from aqueous electrolytes containing high acetate concentrations." Surface & Coatings Technology, 324, 1 (2017).
- 22. S. N. Hasan, M. Xu. and E. Asselin, "Electrosynthesis of metallic molybdenum from water deficient solution containing molybdate ions and high concentrations of acetate." Surf. Coat. Technol., 357, 567 (2019).

  23. L. Suo et al., "Water-in-salt' electrolyte makes aqueous sodium-ion battery safe,
- green, and long-lasting.." Adv. Energy Mater., 7, 1701189 (2017)
- 24. L. Suo, O. Borodin, T. Gao, M. Olguin, J. Ho, X. Fan, C. Luo, C. Wang, and K. Xu, "Water-in-salt' electrolyte enables high-voltage aqueous lithium-ion chemistries.." Science, 350, 938 (2015).
- 25. L. Suo, Y.-S. Hu, H. Li, M. Armand, and L. Chen, "A new class of solvent-in-salt electrolyte for high-energy rechargeable metallic lithium batteries." Nat. Commun., 4, 1481 (2013).
- 26. M. Amiri and D. Bélanger, "Physicochemical and electrochemical properties of water-in-salt electrolytes." ChemSusChem, 14, 2487 (2021).
- 27. J. Zheng et al., "Understanding thermodynamic and kinetic contributions in expanding the stability window of aqueous electrolytes." *Chem*, **4**, 2872 (2018).
- 28. X. Tian, Q. Zhu, and B. Xu, "Water-in-salt' electrolytes for supercapacitors: a review." ChemSusChem, 14, 2501 (2021).
- 29. Q. Huang and T. W. Lyons, "Electrodeposition of rhenium with suppressed hydrogen evolution from water-in-salt electrolyte." Electrochem. Commun., 93, 53 (2018).
- 30. S. De, W. D. Sides, T. Brusuelas, and Q. Huang, "Electrodeposition of superconducting rhenium-cobalt alloys from water-in-salt electrolytes." J. Electroanal. Chem., 860, 113889 (2020).
- 31. B. Malekpouri, K. Ahammed, and Q. Huang, "Electrodeposition and superconductivity of rhenium-iron alloy films from water-in-salt electrolytes." J. Alloys Compd., 912, 165077 (2022).
- 32. M. Amiri and D. Bélanger, "Zinc electrodeposition in acetate-based water-in-salt electrolyte: experimental and theoretical studies." ChemElectroChem, 8, 2737
- 33. J. Han, H. Zhang, A. Varzi, and S. Passerini, "Fluorine-free water-in-salt electrolyte for green and low-cost aqueous sodium-ion batteries." ChemSusChem, 11, 3704 (2018).
- 34. L. Suo et al., "Water-in-salt' electrolyte makes aqueous sodium-ion battery safe, green, and long-lasting." Adv. Energy Mater., 7, 1701189 (2017).
- 35. J. Zhao, Y. Li, X. Peng, S. Dong, J. Ma, G. Cui, and L. Chen, "High-voltage Zn/ LiMn0.8Fe0.2PO4 aqueous rechargeable battery by virtue of 'water-in-salt' electrolyte." Electrochem. Commun., 69, 6 (2016).
- Y. Sui et al., "The influence of ions on the electrochemical stability of aqueous electrolytes." Angew. Chem. Int. Ed., 63, e202401555 (2024).
- 37. M. Pourbaix, Atlas of Electrochemical Equilibria in Aqueous Solutions (Pergamon, Oxford) (1966).
- S. De, J. White, T. Brusuelas, C. Patton, A. Koh, and Q. Huang, "Electrochemical behavior of protons and cupric ions in water in salt electrolytes with alkaline metal chloride." Electrochim. Acta, 338, 135852 (2020).
- 39. M. Amiri and D. Bélanger, "Physicochemical and electrochemical characterization of salt-in-water and water-in-salt potassium and lithium acetate electrolytes." J. Mater. Chem. A, 9, 24012 (2021).
- 40. S. Chen, R. Lan, J. Humphreys, and S. Tao, "Effect of cation size on alkali acetatebased 'water-in-bisalt' electrolyte and its application in aqueous rechargeable lithium battery." Applied Materials Today, 20, 100728 (2020).
- 41. NIST X-ray Photoelectron Spectroscopy Database, (2000), NIST X-ray Photoelectron Spectroscopy Database, NIST Standard Reference Database Number 20, National Institute of Standards and Technology, Gaithersburg MD, 20899 (2000), https://dx.doi.org/10.18434/T4T88K.